Research Square

Preprints are preliminary reports that have not undergone peer review.
They should not be considered conclusive, used to inform clinical practice,
or referenced by the media as validated information.

Glucose/pH-responsive BSA@GOx@MnO_2 nanocascade particles for in vitro regulation of infected diabetic wound microenvironments

Zijie Wu
Nanfang Hospital
Shuyi Yang
Nanfang Hospital
Yuexin Cao
Nanfang Hospital
Liuwen Chen
Nanfang Hospital
Huimin Lin
Southern Medical University
Meng Yu
Southern Medical University
Qi Liu
liuqi@gdpu.edu.cn

Nanfang Hospital

Research Article

Keywords: diabetic wound, infected microenvironment, glucose oxidase, manganese dioxide nanozyme, cascade catalysis, BSA@GOx@MnO_2

Posted Date: November 24th, 2026

DOI: https://doi.org/10.21203/rs.3.rs-11621149/v1

License: This work is licensed under a Creative Commons Attribution 4.0 International License.
Read Full License

Additional Declarations: No competing interests reported.

Glucose/pH-responsive BSA@GOx@MnO_2 nanocascade particles for in vitro regulation of infected diabetic wound microenvironments

Zijie Wu[ab†], Shuyi Yang [ab†], Yuexin Cao[ab†], Liuwen Chen[a], Huimin Lin[c], Meng Yu[c*] and Qi Liu[ad*]

a) Department of Stomatology, Nanfang Hospital, Southern Medical University, Guangzhou, China.

b) School of Stomatology, Southern Medical University, Guangzhou, China.

c) NMPA Key Laboratory for Research and Evaluation of Drug Metabolism & Guangdong Provincial Key Laboratory of New Drug Screening & Guangdong-Hongkong-Macao Joint Laboratory for New Drug Screening, School of Pharmaceutical Sciences, Southern Medical University, Guangzhou, China.

d) Department of Stomatology, The First Affiliated Hospital of Guangdong Pharmaceutical University, Guangzhou, China.

† These authors contributed equally to this work.

* Corresponding authors. E-mail: Qi Liu: liuqi@gdpu.edu.cn; Meng Yu: yumeng999@smu.edu.cn.

Abstract

The repair of infected diabetic wounds is persistently constrained by hyperglycemia, hypoxia, and bacterial colonization, which are mutually reinforcing and cannot be simultaneously corrected by a single antibacterial or oxygen-supplying strategy. To address this challenge, we constructed BSA@GOx@MnO_2 nanocascade particles (BGM NPs) that use endogenous glucose and the weakly acidic environment of diabetic wounds as reaction-triggering signals. In this system, glucose oxidase (GOx) first consumes excess glucose to generate gluconic acid and H_2O_2, which further activates the responsive degradation and enzyme-like catalytic reactions of MnO_2, enabling the generation of antibacterial reactive oxygen species (ROS) while replenishing local oxygen. Thus, BGM NPs couple glucose depletion, bacterial inhibition, and oxygen supplementation into a continuous microenvironment-regulating pathway, reducing the survival advantage of bacteria and alleviating cellular hypoxia to create more favorable conditions for fibroblast migration and wound repair. The main innovation of this design is that lesion-intrinsic metabolic features drive a closed-loop cascade reaction, allowing infection control and pro-repair microenvironment remodeling without external stimulation and providing a new in vitro proof-of-concept platform for treating infected diabetic wounds.

Keywords: diabetic wound; infected microenvironment; glucose oxidase; manganese dioxide nanozyme; cascade catalysis; BSA@GOx@MnO_2

1. Introduction

Diabetes mellitus is a systemic metabolic disease characterized primarily by persistent hyperglycemia, and its prevalence continues to rise, with recent reports estimating a global prevalence of approximately 14%(*1*). Chronic wounds associated with diabetes are particularly prone to delayed healing, and this impaired repair is not caused by a single factor but by the combined effects of hyperglycemia, hypoxia, bacterial infection, oxidative stress, and sustained inflammation. A persistently high-glucose environment not only weakens repair-related fibroblast functions, including migration, proliferation, and collagen deposition, but also provides favorable conditions for the proliferation and biofilm formation of pathogens such as Staphylococcus aureus (*S. aureus*); bacterial colonization further aggravates local inflammation and reduces the efficacy of anti-infective therapy. At the same time, diabetic wounds are often accompanied by microcirculatory dysfunction and tissue hypoxia, which interfere with normal inflammatory resolution, angiogenesis, and tissue remodeling, ultimately leaving wounds in a state of chronic inflammation and stalled repair(*2-6*). Current treatments, including surgical debridement, antibiotic therapy, hyperbaric oxygen therapy, and moist dressings(*7*), can improve the wound environment or control infection to some extent, but they usually act on a single pathological process and struggle to synchronously address hyperglycemia-induced bacterial proliferation, sustained inflammation, local hypoxia, and impaired repair-cell function. Therefore, developing a therapeutic system that responds to the features of infected diabetic wounds and integrates anti-infective activity with pro-repair microenvironment regulation remains of substantial research value.

To address these therapeutic challenges, this study designed a treatment system based on the key limiting factors of infected diabetic wounds and selected functional components capable of microenvironment regulation. Because excess glucose in the wound is both a defining feature of the diabetic pathological microenvironment and a key driver of bacterial overgrowth and repair impairment, we first introduced glucose oxidase (GOx) to consume local glucose and convert it into gluconic acid and H_2O_2, thereby reducing the adverse effects of hyperglycemia on infection expansion and tissue repair at the source(*8, 9*). However,

the catalytic process of GOx consumes oxygen, and GOx alone may further aggravate wound hypoxia. Because nanozymes can further catalyze the GOx metabolite H_2O_2 to generate bactericidal ROS and participate in oxygen generation, we selected MnO_2 nanozyme as the carrier for GOx and as the core component of the cascade reaction(*10, 11*). MnO_2 can undergo responsive degradation in a weakly acidic microenvironment and release Mn^{2+}, while also using GOx-derived H_2O_2 to generate ROS and O_2, thereby coupling glucose consumption, bacterial inhibition, and local oxygen supplementation into a continuous therapeutic process(*12, 13*). Bovine serum albumin (BSA) was further introduced as a stabilizer and chelating carrier to improve the dispersibility, biocompatibility, and delivery stability of the nanoparticles. On this basis, we constructed BSA@GOx@MnO_2 nanocascade particles (BGM NPs) to initiate an endogenous cascade reaction under the high-glucose and weakly acidic conditions of infected diabetic wounds, with the aim of reducing glucose levels, suppressing bacteria in the infected microenvironment, and promoting local oxygen generation to create a more favorable microenvironment for fibroblast migration and wound repair.

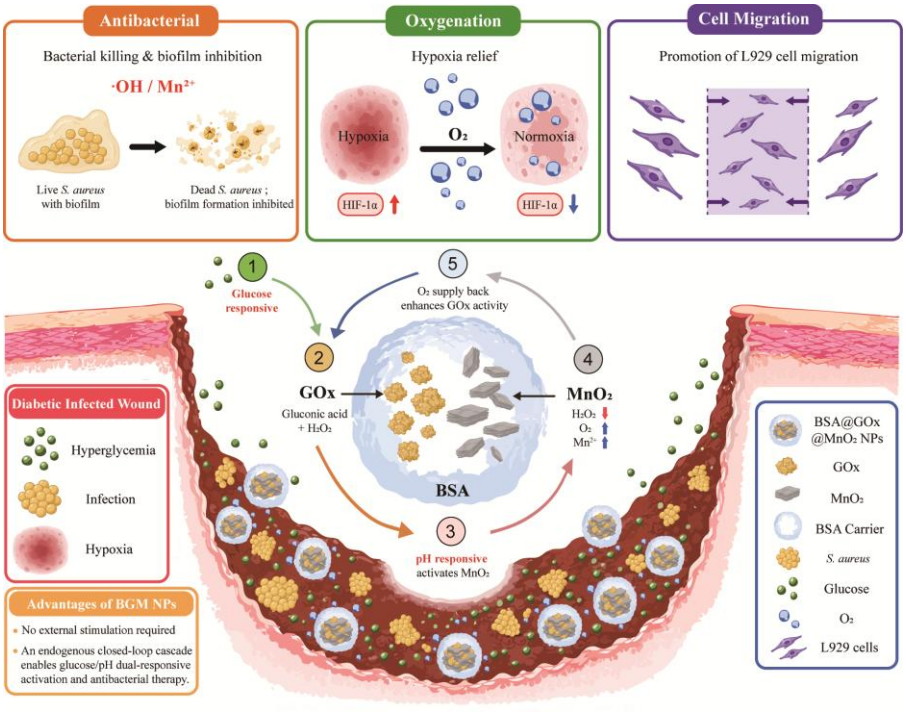


Fig. 1 Schematic illustration of BGM NP synthesis and the proposed glucose/pH-responsive cascade coupling glucose depletion, antibacterial activity and partial mitigation of oxygen depletion under diabetic wound-like conditions.

2. Materials and Methods

2.1 Preparation of BSA@GOx@MnO_2 NPs (BGM NPs)

Glucose oxidase (GOx) was dissolved in ultrapure water to prepare a 5 mg/mL stock solution and stored at 4 °C. $MnCl_2·4H_2O$ solution was added to a bovine serum albumin (BSA) solution containing GOx, and after vigorous shaking for 5 min, NaOH solution was rapidly added dropwise to adjust the pH to 11-12; the reaction solution turned dark brown and was magnetically stirred for another 2 h. The product was then dialyzed against ultrapure water for 2 h to obtain the BGM NP dispersion. BM NPs were prepared using the same procedure except that GOx was omitted. All materials were stored at 4 °C and subjected to ice-bath ultrasonication for 180 s before use to ensure complete dispersion.

2.2 Characterization of BGM NPs

Ultrasonically dispersed BM NP and BGM NP dispersions (1.5 mL) were acid-digested, and the Mn content was determined by inductively coupled plasma mass spectrometry (ICP-MS). The yield was calculated as the ratio between the ICP-MS-measured Mn amount and the input amount of $MnCl_2·4H_2O$ used during synthesis. After ultrasonication, BM NP and BGM NP dispersions were frozen at -80 °C for 24 h and vacuum freeze-dried for 20 h. The dried powder samples were analyzed by Fourier-transform infrared spectroscopy (FT-IR) to assess their molecular structure. Freeze-dried BM NP and BGM NP samples were also analyzed by X-ray photoelectron spectroscopy (XPS). The testing conditions were as follows: monochromatic Al Kα source (E = 1486.68 eV), voltage of 12 kV, current of 6 mA, and vacuum below 10^{-8} mbar. The pass energy was 150 eV for survey spectra and 30 eV for high-resolution spectra.

2.3 Glucose/pH Dual-Responsiveness of BGM NPs

BM NP and BGM NP dispersions (1.5 mL) were separately loaded into dialysis bags (MWCO 3500 Da), placed in centrifuge tubes containing buffers with different pH values (pH 7 and 6), and incubated at 37 °C on a shaker at 180 rpm. At 0, 2, 4, 6, 8, 12, 24, and 48 h, 1.5 mL of the external dialysis solution was collected and

replaced with an equal volume of fresh buffer for subsequent Mn^{2+} and glucose assays. The Mn^{2+} concentration at each time point was determined by ICP-MS, and cumulative release curves were plotted to evaluate pH-responsive release behavior. Residual glucose in the dialysis solution was measured using the hexokinase method with a glucose assay kit (Nanjing Jiancheng). The assay was performed according to the manufacturer's instructions, absorbance at 340 nm was measured using a microplate reader, and the glucose consumption rate was calculated to evaluate the glucose-consuming ability of the materials under different conditions.

2.4 Enzyme-like Activity of BGM NPs

BM NP and BGM NP dispersions were dialyzed as described above, and the external dialysis solution was collected at 0, 2, 4, 6, 8, 12, 24, and 48 h to measure H_2O_2 and ·OH levels. For H_2O_2 detection, an Elabscience hydrogen peroxide colorimetric assay kit was used to prepare a standard curve according to the manufacturer's instructions, and 40 μL of each sample was measured at 405 nm to calculate H_2O_2 concentration and plot the generation curve. For ·OH detection, an Addison hydroxyl radical assay kit was used, absorbance at 532 nm was measured, and ·OH content was calculated. Changes in dissolved oxygen were monitored using a dissolved oxygen meter (ST-8210+). BM NP or BGM NP dispersion was mixed with glucose at a final concentration of 10 mM in a total volume of 5 mL, and the dissolved oxygen concentration of the system was recorded over time.

2.5 Bacterial Experiments with BGM NPs

A two-fold dilution assay was performed in 96-well plates. The materials were serially diluted in MHB medium to final concentrations of 0-16 μg/mL. The *S. aureus* suspension was adjusted to OD_{600} = 0.09 (approximately 1×10^8 CFU/mL) and diluted with MHB containing 10 mM glucose or glucose-free MHB to 1×10^6 CFU/mL. Each well received 50 μL of bacterial suspension and 50 μL of material dilution, yielding a final volume of 100 μL and a final bacterial concentration of 5×10^5 CFU/mL. Vancomycin (2 μg/mL) was used as a positive control (based on the Clinical and Laboratory Standards Institute susceptibility breakpoint of ≤2

μg/mL for *S. aureus*), and growth-control wells (bacterial suspension + MHB) and negative-control wells (MHB) were included. After static incubation at 37 °C for 20 h, OD_{600} was measured. The experiment was repeated three times, with four replicate wells per group. For the plate-spreading assay, clear and non-turbid wells from the Minimum Inhibitory Concentration (MIC) assay were mixed by pipetting, and 50 μL aliquots were spread onto MHA plates followed by incubation at 37 °C for 48 h. The lowest material concentration with fewer than 3 CFU per plate was defined as the Minimum Bactericidal Concentration (MBC).

In 24-well plates, BGM was co-cultured with *S. aureus* suspension containing 10 mM glucose (5×10^5 CFU/mL) for 20 h in a total volume of 500 μL per well. The supernatant was discarded, the wells were washed three times with PBS, and 500 μL of 0.1% crystal violet was added to each well for 15 min of staining. After removing the staining solution, the wells were washed three times with PBS, air-dried at room temperature, and treated with 1 mL of 30% glacial acetic acid to dissolve the crystal violet. The supernatant was collected and absorbance at 550 nm was measured, with 30% glacial acetic acid used as the blank control, to quantify biofilm formation.

BGM NPs (2.5 μg/mL) were co-cultured with *S. aureus* (1×10^6 CFU/mL) for 4 h. The staining solution was prepared according to the instructions of the SYTO-9/PI kit, and bacterial suspensions were stained for 15 min at room temperature in the dark before slide preparation. Samples were observed under a fluorescence microscope, with green fluorescence indicating live bacteria and red fluorescence indicating dead bacteria. ImageJ was used to calculate fluorescence-covered area and total fluorescence intensity, which were normalized to the growth control set as 100%; intergroup comparisons were performed using the t-test (alpha = 0.05).

2.6 Cellular Experiments with BGM NPs

L929 cells in logarithmic growth phase were seeded into 96-well plates at 8×10^3 cells per well. After 24 h of adhesion, the original medium was removed and replaced with DMEM containing different concentrations (0, 0.5, 1, 1.5, 2, 2.5, 3, 4, 6, and 8 μg/mL) of GOx, BM NPs, or BGM NPs, supplemented with 10% FBS and 10 mM

glucose, at 100 μL per well with three replicate wells per group. Edge wells were filled with PBS. The plates were placed in anaerobic bags containing anaerobic indicators and cultured at 37 °C. After 24 h of culture, the supernatant was removed, serum-free DMEM containing 10% Cell Counting Kit-8 (CCK-8) was added at 100 μL per well, and the plates were incubated at 37 °C for 1 h in the dark before absorbance at 450 nm was measured. Cell viability (%) was calculated as $(OD_{experimental} - OD_{blank}) / (OD_{control} - OD_{blank}) \times 100\%$.

L929 cells were seeded into 6-well plates at 5×10^5 cells per well and, after reaching 90% confluence, were switched to serum-free medium overnight. A scratch was created using a 10 μL pipette tip, followed by three washes with PBS. DMEM containing Control, GOx, BM NPs, or BGM NPs, supplemented with 1% FBS and 10 mM glucose, was then added at a final drug concentration of 2.5 μg/mL in a total volume of 2 mL. The plates were placed in anaerobic bags containing anaerobic indicators and cultured at 37 °C. Images were captured at 0, 24, and 48 h, scratch width was measured using ImageJ, and the healing rate was calculated as (width at 0 h - width at the measured time point)/width at 0 h x 100%. The experiment was repeated three times.

L929 cells were seeded into 6-well plates at 5×10^5 cells per well and cultured to 90% confluence before being switched to serum-free medium overnight. Drug-containing medium was added according to group allocation (Control, GOx, BM NPs, and BGM NPs), with a final drug concentration of 2.5 μg/mL and Mn content of 7.7 μM, followed by 24 h of anaerobic culture. Total RNA was extracted using the Trizol method, and RNA concentration and purity were measured using Nanodrop. A total of 1 ug RNA was reverse-transcribed into cDNA, and qPCR was performed using the SYBR Green method. Primer sequences were verified by NCBI BLAST. The reaction conditions were 95 °C for 5 min, followed by 45 cycles of 95 °C for 10 s and 60 °C for 30 s. Relative HIF-1α expression was calculated using the 2^-ΔΔCt method, and statistical analysis was performed in GraphPad Prism.

L929 cells were seeded into 6-well plates at 5×10^5 cells per well, cultured for 24 h, and then switched to serum-free medium overnight. Under anaerobic conditions, drug-containing medium was added at a final drug concentration of 2.5 μg/mL and Mn content of 7.7 μM, and the cells were cultured for another 24 h. All

subsequent steps were performed on ice: after PBS washing, RIPA lysis buffer containing protease inhibitors was added, lysates were collected, centrifuged at 13,000 g for 20 min at 4 °C, and the supernatant was collected. Protein concentration was determined by the BCA method, loading buffer was added, and proteins were denatured at 100 °C for 10 min. After SDS-PAGE and membrane transfer, membranes were blocked and incubated with primary antibodies against HIF-1α and the internal reference, followed by secondary antibody incubation and signal development. Band grayscale values were quantified using ImageJ, and one-way analysis of variance was performed in GraphPad Prism.

3. Results and Discussion

3.1 Synthesis and Characterization of BGM NPs

We first prepared BSA@GOx@MnO_2 nanocascade particles (BGM NPs) using a BSA-mediated biomineralization strategy, with BM NPs prepared without GOx as the control to determine whether GOx introduction affected MnO_2 formation. Macroscopic observation showed that BGM NPs were well dispersed in MHB, DMEM, PBS, and water, and all dispersions remained stable after standing at room temperature for 2 h without obvious precipitation, suggesting good short-term dispersion stability in the subsequent bacterial and cellular experimental systems (Fig. 2A). ICP-MS showed that the average manganese loading of BGM NPs was 90.5%, close to the 94.72% observed for BM NPs, indicating that GOx addition did not markedly reduce manganese incorporation efficiency (Fig. 2B). FT-IR spectra showed characteristic peaks associated with Mn-O bonds in the 415-518 cm^{-1} range, and XPS showed Mn 2p3/2 and Mn 2p1/2 main peaks at approximately 642 eV and 654 eV, respectively, further supporting the formation of MnO_2 structures (Fig. 2C, E). TEM images revealed that BGM NPs had a nearly spherical nanoparticle morphology with good dispersibility (Fig. 2D). DLS analysis showed that the average hydrodynamic radii (Rh) of BGM NPs and BM NPs were 267.2 nm and 50.97 nm, respectively. The larger hydrodynamic radius of BGM NPs compared with BM NPs suggested that GOx/BSA/MnO_2 complexation formed complete nanocascade particles, further supporting the successful construction of BGM NPs (Fig. 2F).

These characterization results indicate that BSA functions as a stabilizer in this system and provides a mild biocompatible interface for the co-assembly of GOx and MnO_2. Previous studies have shown that albumin nanoparticles are commonly used to construct multifunctional nanodelivery platforms because of their good biocompatibility, abundant functional groups, and capacity for drug or ion binding(*14*). Meanwhile, metal oxide nanozymes such as MnO_2 possess tunable redox activity and enzyme-like catalytic capacity and are important components for constructing responsive materials that regulate pathological microenvironments(*15*). Therefore, the BGM NPs in this study are not a simple mixture of GOx, BSA, and MnO_2, but rather a BSA-stabilized nanostructure that integrates a glucose-responsive component and an enzyme-like catalytic component into a single platform, providing the structural basis for subsequent cascade reactions.

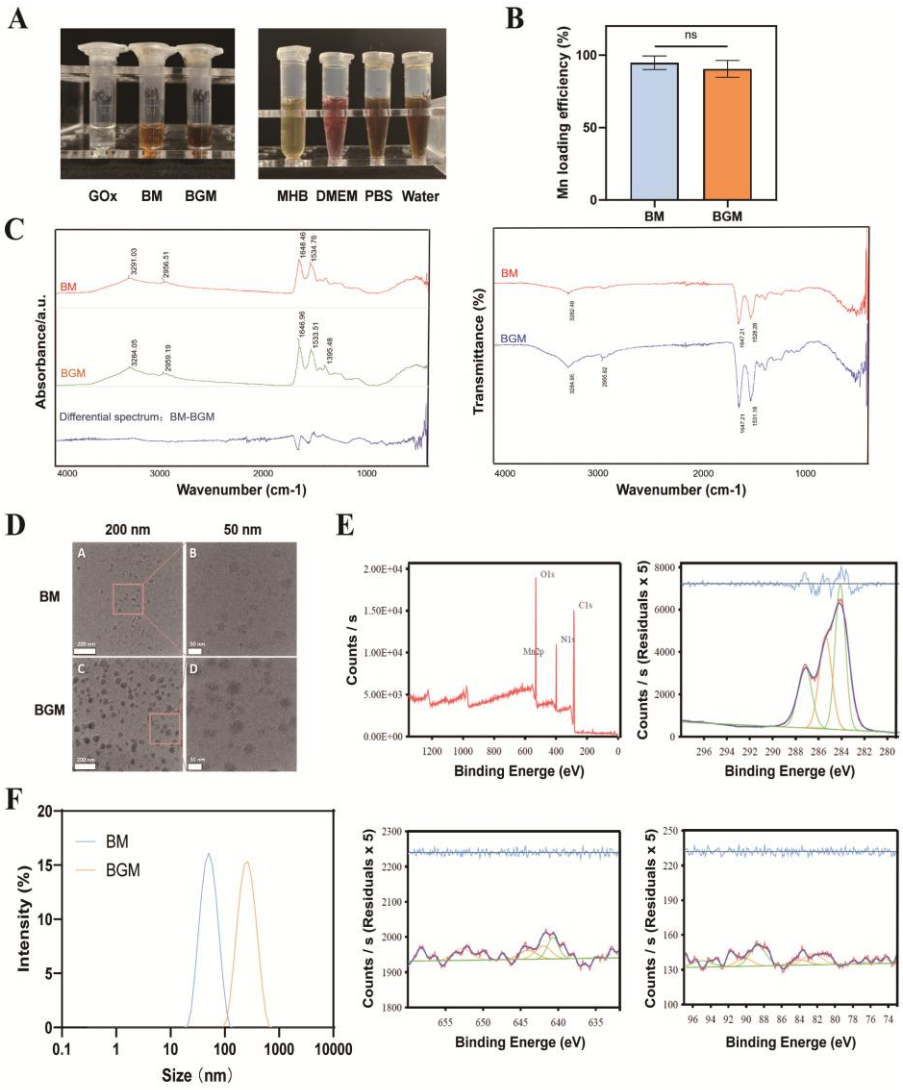


Fig. 2 Material synthesis and characterization of BGM NPs

(A) Photographs showing material dispersion in MHB, DMEM, PBS, and water. (B) ICP-MS quantification of manganese content. (C) FT-IR absorbance spectra. (D) TEM characterization of BM and BGM NP morphology (scale bar = 200 nm, 50nm). (E) XPS analysis of the elemental composition and valence states of BGM NPs. (F) DLS measurement of particle size.

3.2 Glucose/pH Dual-Responsiveness and Enzyme-like Catalytic Properties of BGM NPs

To evaluate whether BGM NPs can specifically respond to the diabetic wound microenvironment and to investigate their glucose/pH dual-responsive properties, we prepared neutral and weakly acidic solutions with or without glucose to simulate the physiological conditions of normal tissue and diabetic wounds, and examined Mn^{2+} release and glucose consumption by BGM NPs under these conditions over 48 h. The results showed that BM NPs were relatively stable at pH 7 under glucose-free conditions, and more than 90% of MnO_2 remained even after glucose addition; in contrast, the cumulative Mn^{2+} release percentage of BGM NPs increased in the acidic environment at pH 6. When acidity and glucose were present together, the cumulative Mn^{2+} release rate of the BGM NP group almost reached 100% by the end of the experiment. These results verified that BGM NPs possess glucose/pH dual-responsiveness and can use environmental glucose to initiate the cascade reaction (Fig. 3A, B). Meanwhile, BGM NPs consumed glucose and generated H_2O_2, further promoting ·OH production. ROS-generation curves showed no obvious difference in H_2O_2-generating capacity between BGM NPs and GOx, while BGM NPs also efficiently generated the ROS species ·OH (Fig. 3C, D). Dissolved oxygen monitoring was used to determine the catalase-like catalytic activity of the materials, and the results showed that GOx alone markedly consumed oxygen in the system, whereas dissolved oxygen levels were higher in the BGM NP group than in the GOx group, suggesting that MnO_2 partially compensates for oxygen consumption caused by the GOx reaction (Fig. 3E).

The core of this study lies in the design specificity of the material system for diabetic wounds. First, GOx and MnO_2 form a closed cascade circuit at the nanoscale: gluconic acid produced by GOx-catalyzed glucose oxidation creates a local acidic microenvironment that activates the catalytic activity of MnO_2, whereas O_2 generated from MnO_2-mediated H_2O_2 decomposition replenishes the oxygen consumed by GOx catalysis, thereby avoiding the contradiction that GOx alone may aggravate local hypoxia and ultimately enabling self-regulated closed-loop cascade operation. Notably, previous studies have used GOx or nanozymes to construct glucose-responsive cascade systems, demonstrating that lesion glucose can serve as endogenous reaction fuel for the treatment of diabetic infection or chronic wounds. For example, the glucose-powered

activatable nanozyme reported by Chen *et al*. uses the GOx reaction to improve local pH and H_2O_2 conditions, thereby enhancing nanozyme antibacterial activity(*16*); Du *et al*. proposed pH-switchable nanozyme cascade catalysis for spatiotemporal modulation of hyperglycemia, infection, hypoxia, and oxidative stress in diabetic ulcers(*17*). The BGM NPs in this study are consistent with these strategies but place greater emphasis on the substrate-relay relationship between GOx and MnO_2. In this way, glucose is not only a pathological factor in diabetic wounds but also an endogenous signal that initiates the antibacterial and oxygen-supplying functions of the material. Through the BSA-mediated integration strategy, glucose responsiveness (GOx), catalytic oxygen production and chemodynamic antibacterial activity (MnO_2), and controllable Mn^{2+} delivery (BSA) are unified within a single nanoplatform, fundamentally avoiding the complexity and risks of stepwise administration of multiple components. Second, BGM NPs rely entirely on endogenous signal responsiveness, using the high local glucose concentration in wounds as the trigger switch; unlike catalytic materials that require external stimulation such as NIR-II irradiation, this design requires no near-infrared light, photothermal activation, photodynamic activation, or other external physical stimulus, thereby substantially reducing dependence on specialized equipment and giving it particular translational potential for chronic diabetic wound management(*18*).

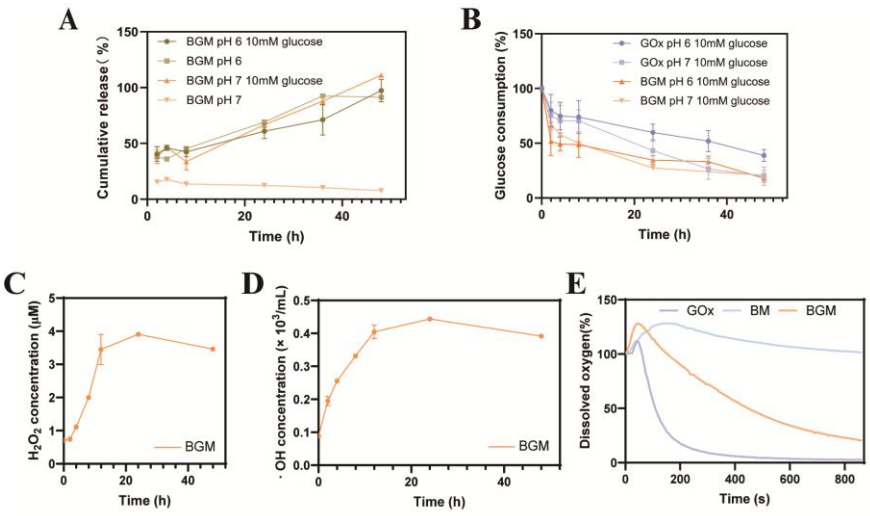


Fig. 3 Dual-responsive activation and peroxidase-like properties of BGM NPs

(A) Glucose-responsive Mn ion release from BGM NPs. (B) pH-dependent changes in glucose consumption in GOx- and BGM-containing systems initially supplemented with 10 mM glucose. (C) Dual-responsive H_2O_2 generation by BGM NPs. (D) Dual-responsive ·OH generation by BGM NPs. (E) Dissolved oxygen meter analysis of the effects of different materials on dissolved oxygen in a high-glucose neutral environment. Data are mean ± SD, n = 3; *p < 0.05, **p < 0.01, ***p < 0.001; ns, not significant.

3.3 BGM NPs Effectively Inhibit Bacterial Colonization in Diabetic Wounds

We selected *S. aureus*, a major pathogen in infected diabetic wounds, to evaluate the antibacterial activity of BGM NPs. First, we investigated the growth characteristics of *S. aureus* by measuring the optical density of bacterial suspensions at 600 nm (OD_{600}) and selected the linear growth phase for subsequent experiments. The microplate two-fold dilution assay showed that, in the absence of additional glucose, neither GOx nor BGM NPs exhibited obvious antibacterial effects; under 10 mM glucose, however, the MIC of BGM NPs was 1.0 μg/mL, which was half that of the GOx group (2.0 μg/mL) (Fig. 4A, C). Vancomycin at 2 μg/mL was used as the positive control and BGM NPs achieved an antibacterial effect close to that of the positive control at 1.0 μg/mL (Fig. 4D), indicating high antibacterial efficiency under glucose-triggered conditions. The plate-spreading assay further showed that the MBC of BGM NPs (1.0 μg/mL) and GOx (2.0 μg/mL) were consistent with the MIC (Fig. 4E), indicating that BGM NPs not only inhibited *S. aureus* growth but also exerted bactericidal activity in glucose-containing environments. By contrast, BM NPs showed no obvious antibacterial activity under either glucose-containing or glucose-free conditions (Fig. 4B).

These results indicate that the antibacterial activity of BGM NPs depends on glucose triggering and is stronger than that of GOx alone. This may be because H_2O_2 generated by the GOx reaction is further converted by MnO_2 into ROS such as ·OH, thereby enhancing oxidative damage to bacteria. Antibacterial nanomaterials commonly act through membrane disruption, oxidative stress, metal-ion interference, and multi-target metabolic injury, a multi-target antibacterial mode distinct from the killing mechanism of conventional antibiotics that depend on specific molecular targets(*19*). Previous studies have inhibited drug-

resistant bacteria and their biofilms by combining nanozyme peroxidase-like activity with near-infrared photothermal effects(*20, 21*). In comparison, the antibacterial advantage of BGM NPs arises from the material's own chemodynamic effects and peroxidase-like activity, allowing bacterial killing without any auxiliary external intervention. The antibacterial advantage of BGM NPs lies in the glucose-driven cascade bactericidal process formed under high-glucose infected conditions, which converts the hyperglycemic burden into reaction fuel for antibacterial activity and makes the antibacterial response more compatible with the lesion microenvironment. BGM NPs may also further enhance antibacterial effects through Mn^{2+} release, and this multiple ROS-mediated bactericidal mode does not rely on the action pathways of conventional antibiotics, providing an alternative strategy for addressing the increasingly severe problem of bacterial resistance(*22, 23*).

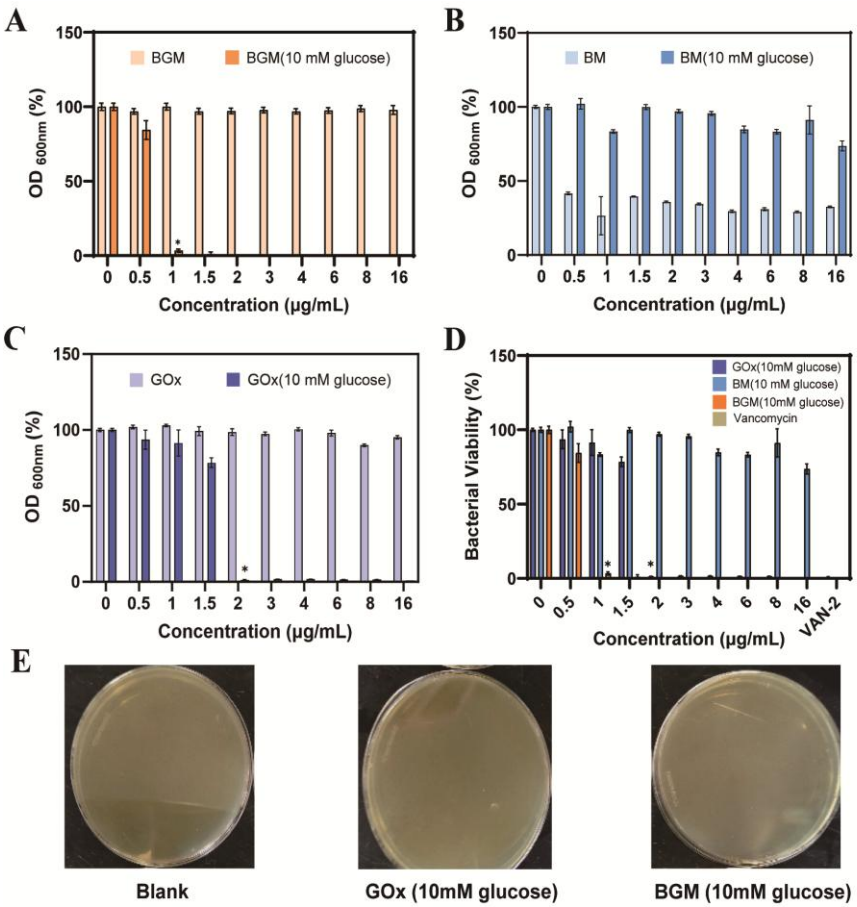


Fig. 4 Antibacterial activity of BGM NPs

(A-D) Antibacterial results and summary data (D) for different concentrations of A, BGM; B, BM; and C, GOx in MHB containing 0 or 10 mM glucose. (E) Plate-spreading assay identifying the MBC concentration. Data are mean ± SD, n = 3; *p < 0.05, **p < 0.01, ***p < 0.001; ns, not significant.

3.4 BGM NPs Inhibit Bacterial Biofilm Formation in Diabetic Wounds

To further evaluate the ability of BGM NPs to intervene in infection progression, we used crystal violet staining to assess their effect on *S. aureus* biofilm formation and SYTO-9/PI live/dead staining to observe bacterial viability. The results showed that BGM NPs at both 2 and 3 μg/mL markedly inhibited *S. aureus* biofilm formation after 24 and 48 h, with effects close to those of vancomycin, whereas neither GOx nor BM NPs produced significant antibiofilm activity under the tested conditions (Fig. 5A). Live/dead fluorescence staining showed that, after 4 h of BGM NP treatment under high-glucose conditions, PI-positive bacterial signals increased, while the total fluorescence intensity and fluorescence-covered area significantly decreased relative to the growth control, suggesting reduced bacterial viability and bacterial coverage (Fig. 5B–D).

Biofilms are an important contributor to the long-term non-healing of infected diabetic wounds. Chronic diabetic foot ulcers often contain complex polymicrobial biofilm infections, and biofilms can increase bacterial tolerance to antibiotics and host immune clearance while maintaining a local inflammatory state(*24*). Therefore, treatment of infected diabetic wounds should not focus only on killing planktonic bacteria, but should also block biofilm formation, reduce inflammation, and improve the hypoxic microenvironment(*25*). In this study, the inhibition of biofilm formation by BGM NPs may arise from two sequential steps: first, the high-glucose environment initiates the GOx/MnO_2 cascade reaction to generate ROS that kill planktonic *S. aureus*; second, reduced early bacterial activity decreases subsequent adhesion, aggregation, and biofilm establishment. It should be noted that the present study mainly demonstrates that BGM NPs inhibit the formation of *S. aureus* mono-species biofilms, but it does not directly prove that they

can clear mature polymicrobial biofilms in clinical wounds. Future studies should therefore further verify their antibiofilm capacity using mature biofilm models and polymicrobial infection models.

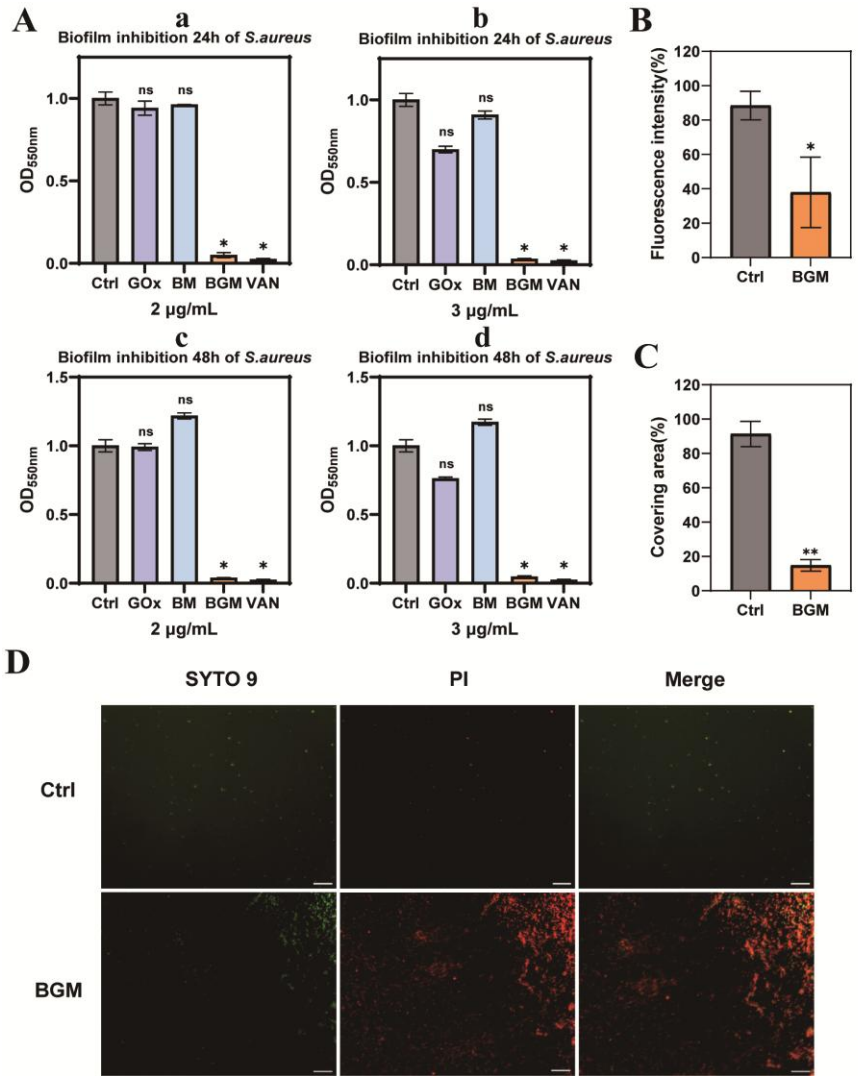


Fig. 5 Antibiofilm activity of BGM NPs

(A) Crystal violet staining analysis of the activity of BGM NPs against *S. aureus* mono-species biofilms after a, 24 h at 2 μg/mL; b, 24 h at 3 μg/mL; c, 48 h at 2 μg/mL; and d, 48 h at 3 μg/mL, compared with controls. (B) Percentage live/dead staining fluorescence intensity. (C) Percentage live/dead staining fluorescence coverage area. (D) Representative live/dead fluorescence staining images. Scale bar, 50 μm. Data are mean ± SD, n = 3; *p < 0.05, **p < 0.01, ***p < 0.001; ns, not significant.

3.5 BGM NPs Accelerate L929 Fibroblast Migration to Promote Diabetic Wound Repair

To evaluate the cytocompatibility and pro-repair potential of BGM NPs, we first used the CCK-8 assay to examine the effects of different material concentrations on L929 fibroblast viability. The results showed that L929 cell viability remained above 80% when the BGM NP concentration was ≤ 6 μg/mL, suggesting good cytocompatibility within this concentration range; when the material concentration increased further, cell proliferation was inhibited to some extent (Fig. 6A). On this basis, we used a scratch assay to observe cell migration. The results showed that scratch closure in the BGM NP-treated group was faster than that in the control group at 24 and 48 h, and quantitative analysis showed an increased scratch closure rate, whereas the BM NP group did not differ markedly from the blank control group (Fig. 6B, C).

Fibroblast migration is a key step in the transition of wounds from the inflammatory phase to the proliferative phase, granulation tissue formation, and extracellular matrix deposition(*26*). Under diabetic conditions, hyperglycemia, infection, persistent inflammation, and hypoxia jointly impair fibroblast migration, proliferation, and collagen deposition, causing wounds to remain in a state of delayed repair(*27*). Previous studies have shown that glucose/ROS-responsive nanozymes can promote fibroblast migration and angiogenesis-related processes by regulating oxidative stress and oxygen balance in diabetic wounds(*28*). Together with the present results, the pro-migratory effect of BGM NPs on L929 cells may not arise from a single factor but from continuous improvement of the microenvironment: GOx consumes glucose and reduces the adverse effects of hyperglycemia on cellular repair; MnO_2 converts H_2O_2 into O_2 and alleviates oxygen consumption caused by the GOx reaction; and ROS-mediated antibacterial activity reduces infectious stimulation, creating more favorable local conditions for fibroblast migration. However, the scratch assay only indicates improvement in the cell-migration phenotype and cannot fully represent in vivo angiogenesis, immune regulation, collagen deposition, or re-epithelialization. Future studies may further examine integrin expression, cytoskeletal rearrangement, mitochondrial function, and oxidative stress levels to clarify the downstream mechanisms by which BGM NPs promote cell migration.

3.6 BGM NPs Alleviate the Cellular Hypoxic Microenvironment of Diabetic Wounds

To verify the ability of BGM NPs to alleviate oxygen consumption associated with the GOx reaction, we combined dissolved oxygen detection, RT-qPCR, and Western blotting to analyze hypoxia-related indicators in L929 cells. Dissolved oxygen measurements showed that GOx alone markedly reduced dissolved oxygen in the system, whereas dissolved oxygen levels were higher in the BGM NP group than in the GOx group. RT-qPCR showed that HIF-1α mRNA expression in L929 cells decreased after BGM NP treatment, whereas HIF-1α mRNA expression levels in the BM NP and GOx groups did not differ significantly from the control group (Fig. 6D); Western blotting further showed that after 24 h of hypoxic culture, HIF-1α protein expression levels increased in the GOx and BM NP groups and differed markedly from the blank control group, whereas HIF-1α protein expression was lower in the BGM NP group than in the control group (Fig. 6D-F). These results indicate that the MnO_2 component in BGM NPs compensates for oxygen consumption caused by GOx catalysis and reduces the cellular hypoxic response.

Hypoxia is an important limiting factor in the impaired repair of chronic and diabetic wounds. In diabetic tissue, hypoxia-induced VEGF expression and angiogenic responses may be impaired, thereby affecting wound perfusion, cell migration, and tissue remodeling(*29*). HIF-1α is an important transcription factor through which cells sense hypoxia and plays an important role in wound repair and fibrosis regulation. However, persistent hypoxia in diabetic wounds does not necessarily translate into effective angiogenesis and tissue repair, and may instead coexist with prolonged inflammation and repair arrest(*30, 31*). Studies of oxygen self-supplying nanozyme hydrogels have noted that GOx-mediated glucose oxidation depends on oxygen; therefore, if oxygen supplementation is absent, the cascade reaction may be limited by the hypoxic environment of diabetic wounds(*32*). In this study, BGM NPs catalyzed H_2O_2 to produce O_2 through MnO_2, thereby effectively compensating for the oxygen-consumption problem associated with GOx alone. This result also explains why BGM NPs showed both antibacterial and pro-migratory effects: rather than acting in isolation to kill bacteria or promote migration, they continuously improve the repair microenvironment experienced by fibroblasts by reducing glucose burden, suppressing bacteria, and alleviating hypoxia.

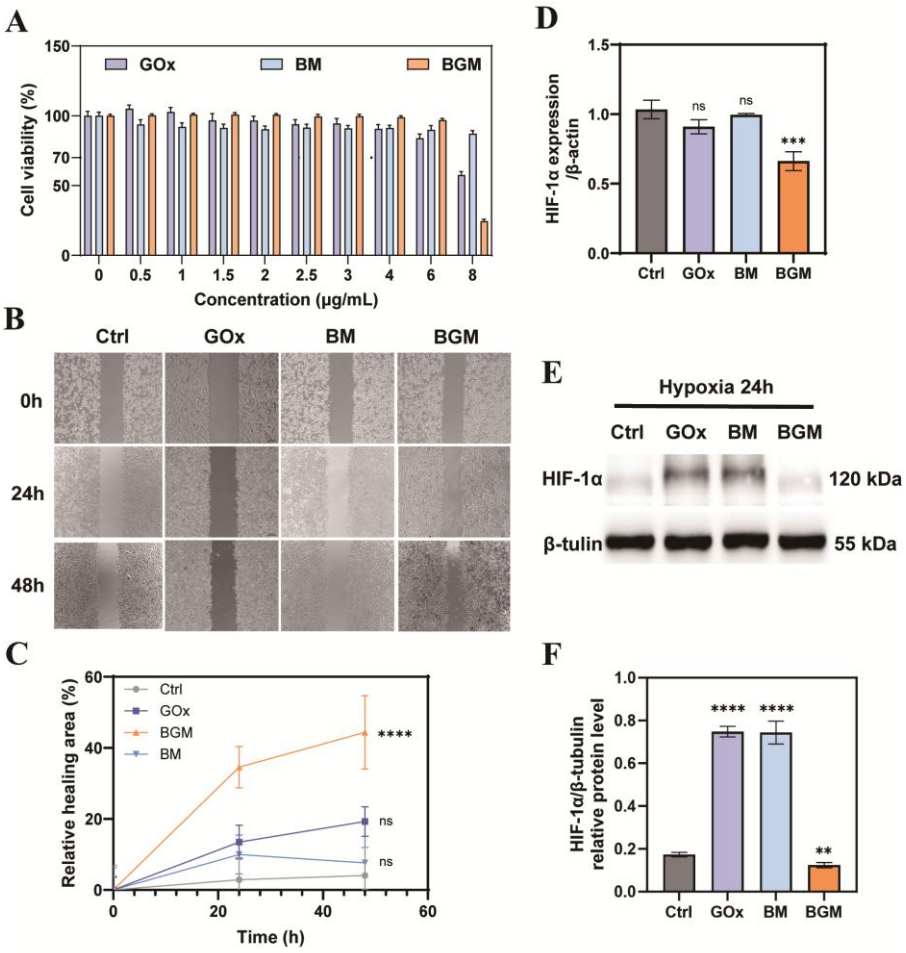


Fig. 6 BGM NPs promote fibroblast migration and alleviate the hypoxic microenvironment in vitro

(A) CCK-8 assay of the biotoxicity of BGM NPs toward L929 cells under high-glucose hypoxic conditions. (B) Scratch assay images of L929 cells stimulated with different materials for 48 h under high-glucose hypoxic conditions. (C) Quantitative analysis of scratch assay images using ImageJ. (D) RT-qPCR analysis of changes in HIF-1α expression in L929 cells after BGM NP treatment. (E) Western blot chemiluminescence images showing the effect of BGM NPs on HIF-1α protein expression under high-glucose hypoxic conditions. (F) ImageJ quantitative analysis of Western blot images. Data are mean ± SD, n = 3; *p < 0.05, **p < 0.01, ***p < 0.001; ns, not significant.

4. Conclusion

This study confirmed the structural basis of BSA@GOx@MnO_2 NPs through material characterization and verified their in vitro function for regulating the infected diabetic wound microenvironment across five functional dimensions: microenvironment responsiveness, enzyme-like catalysis, antibacterial and antibiofilm activity, fibroblast migration, and hypoxia alleviation. The system uses high-glucose and weakly acidic conditions to initiate a cascade reaction in which GOx consumes glucose and generates gluconic acid and H_2O_2, further activating the responsive release and enzyme-like catalytic activity of MnO_2 to achieve ROS-mediated antibacterial activity and local oxygen supplementation. In vitro experiments showed that BGM NPs have good dispersibility and cytocompatibility, effectively inhibit *S. aureus* growth and biofilm formation in glucose-containing environments, alleviate GOx-associated oxygen consumption, downregulate HIF-1α expression in L929 cells, and promote fibroblast migration. These findings indicate that BGM NPs, through a closed-loop cascade reaction fueled by endogenous glucose, couple glucose depletion, antibacterial action, and oxygen supplementation into a continuous microenvironment-modulating pathway that synergistically addresses bacterial infection, local hypoxia, and impaired cellular repair, thereby providing a valuable in vitro proof of concept and experimental basis for microenvironment regulation in infected diabetic wounds. Future studies will focus on deepening mechanistic understanding, advancing formulation translation, and completing in vivo therapeutic evaluation in animal models to accelerate movement toward clinical application.

5. References

1. Collaboration, N.C.D.R.F. (2024) Lancet. 404, 2077-2093.

2. Zheng, Y., et al. (2025) Int Immunopharmacol. 161, 115058.

3. Wang, J., et al. (2023) Front Immunol. 14, 1104890.

4. Singh, N., et al. (2019) Nanoscale. 11, 3855-3863.

5. Zhang, L., et al. (2026) ACS Appl Mater Interfaces. 18, 16069-16084.

6. Matoori, S., A. Veves, and D.J. Mooney. (2021) Sci Transl Med. 13,

7. Winter, G.D. and J.T. Scales. (1963) Nature. 197, 91-2.

8. Shi, M., et al. (2022) Theranostics. 12, 2658-2673.

9. Zeng, Y., et al. (2024) Acta Pharm Sin B. 14, 5037-5052.

10. Zhang, R., K. Fan, and X. Yan. (2020) Sci China Life Sci. 63, 1183-1200.

11. Jia, S., et al. (2025) Int J Nanomedicine. 20, 8783-8810.

12. Tenaud, I., et al. (1999) Br J Dermatol. 140, 26-34.

13. Li, M., et al. (2025) J Med Chem. 68, 17808-17822.

14. An, F.F. and X.H. Zhang. (2017) Theranostics. 7, 3667-3689.

15. Liu, Q., et al. (2021) Nanomicro Lett. 13, 154.

16. Chen, L., et al. (2021) Angew Chem Int Ed Engl. 60, 23534-23539.

17. Du, X., et al. (2022) J Nanobiotechnology. 20, 12.

18. Shan, J., et al. (2023) Acta Biomater. 157, 200-209.

19. Xie, M., et al. (2023) Angew Chem Int Ed Engl. 62, e202217345.

20. Yao, M., et al. (2025) Small. 21, e06681.

21. Lin, K., et al. (2026) J Control Release. 392, 114653.

22. Calabrese, G., et al. (2023) Biomater Adv. 145, 213193.

23. Chen, Y., et al. (2025) Colloids Surf B Biointerfaces. 255, 114966.

24. Dowd, S.E., et al. (2008) PLoS One. 3, e3326.

25. Tu, C., et al. (2022) Biomaterials. 286, 121597.

26. Rodrigues, M., et al. (2019) Physiol Rev. 99, 665-706.

27. Brem, H. and M. Tomic-Canic. (2007) J Clin Invest. 117, 1219-22.

28. Yu, X., et al. (2022) Mater Today Bio. 15, 100308.

29. Thangarajah, H., et al. (2009) Proc Natl Acad Sci U S A. 106, 13505-10.

30. Falanga, V., et al. (2022) Nat Rev Dis Primers. 8, 50.

31. Ruthenborg, R.J., et al. (2014) Mol Cells. 37, 637-43.

32. Li, Y., et al. (2022) Small. 18, e2200165.

6. Statements & Declarations

Funding

This work was supported by National Natural Science Foundation of China (52003112); Guangdong Postgraduate Education Innovation Program (2026ANLK_041); the Research Fund of Nanfang Hospital, Southern Medical University (2023A023); the Higher Medical Education Research Project of Guangdong Pharmaceutical University (GKP202503); the Higher Education Teaching Reform Research Project of the Guangdong Higher Education Teaching Management Association (ZD202601008); and the Undergraduate Innovation and Entrepreneurship Training Program (202610573015, G202604302023).

Competing Interests

The authors declare that they have no known competing financial interests or personal relationships that could have appeared to influence the work reported in this paper.

Author Contributions

Zijie Wu: writing– original draft, data curation, visualization, validation. Shuyi Yang: writing – review & editing, data curation. Yuexin Cao: conceptualization, methodology, investigation, validation. Liuwen Chen: investigation, validation. Huimin Lin: investigation, validation. Meng Yu: writing– review & editing, resources, project administration. Qi Liu: writing– review & editing, resources, supervision, project administration, funding acquisition.

Ethics approval

This study was performed entirely in vitro using the established L929 murine fibroblast cell line and *Staphylococcus aureus*, without involving human participants or animal subjects.

Data availability

All data supporting the findings of this study are available within the paper. Additional data sets or raw experimental data are available from the corresponding author upon reasonable request.